



HAL
open science

How a new strain transformable titanium-based biomedical alloy can be designed for balloon expendable stents

D.M. Gordin, F. Sun, D. Laillé, F. Prima, T. Gloriant

► **To cite this version:**

D.M. Gordin, F. Sun, D. Laillé, F. Prima, T. Gloriant. How a new strain transformable titanium-based biomedical alloy can be designed for balloon expendable stents. *Materialia*, 2020, 10, pp.100638. 10.1016/j.mtla.2020.100638 . hal-02536605

HAL Id: hal-02536605

<https://univ-rennes.hal.science/hal-02536605>

Submitted on 15 Apr 2020

HAL is a multi-disciplinary open access archive for the deposit and dissemination of scientific research documents, whether they are published or not. The documents may come from teaching and research institutions in France or abroad, or from public or private research centers.

L'archive ouverte pluridisciplinaire **HAL**, est destinée au dépôt et à la diffusion de documents scientifiques de niveau recherche, publiés ou non, émanant des établissements d'enseignement et de recherche français ou étrangers, des laboratoires publics ou privés.

How a new strain transformable titanium-based biomedical alloy can be designed for balloon expandable stents

D.M. Gordin¹, F. Sun², D. Laillé¹, F. Prima², T. Gloriant^{1*}

¹Univ Rennes, INSA Rennes, CNRS, Institut des Sciences Chimiques de Rennes – UMR 6226, F-35000 Rennes, France

²PSL Research University, Chimie ParisTech-CNRS, Institut de Recherche de Chimie Paris – UMR 8247, F-75005 Paris, France

*corresponding author: Thierry.Gloriant@insa-rennes.fr

Abstract: Although largely used for numerous medical devices, the current titanium medical grades are not adapted for the manufacture of balloon expandable vascular stents due to their low plastic deformation abilities compared to stainless steels and cobalt-chromium alloys. In this study, a new biocompatible Ti-16Nb-8Mo alloy (wt.%) was designed with the objective to obtain large ductility and high strain hardening. In the alloy, a massive twinning and strain-induced martensitic transformation were observed to accommodate the plastic deformation leading to a very large plastic deformation since more than 45% of elongation at fracture were reached by tensile test. This huge plasticity, unusual for titanium alloys, is due to a complex deformation mechanism implying TWinning Induced Plasticity (TWIP) and Transformation Induced Plasticity (TRIP) effects, which were particularly investigated in such strain transformable alloy by electron backscattering diffraction (EBSD), by transmission electron microscopy (TEM) and by in-situ tensile test under synchrotron beam (SXRD).

Keywords: titanium alloy, plasticity, twinning, martensitic transformation

1. Introduction

Stent technology is being continually advanced, as scientists and engineers pursue ways to develop new devices and better options available for the treatment of patients with cardiovascular diseases. For a good functionality, balloon expandable stents should have the ability to undergo plastic deformation to reach the required size once deployed. Generally, the metals commonly used for manufacturing balloon expandable stents are stainless steels or

cobalt-chromium based alloys due to their high strength, large plastic deformation and strain hardening [1, 2]. However, biocompatibility is an issue with such materials because of their high percentage of nickel and chromium. Indeed, according to previous works on the biocompatibility of various metals, the corrosion behavior of stainless steels and Co-Cr alloys is dominated by their nickel and chromium elements, which may induce redox reaction, hydrolysis and complex metal ion–organic molecule binding reactions, whereas none are observed with titanium [3, 4]. Although titanium alloys, such as the Ti-6Al-4V ELI alloy, are widely used as biomaterials for orthopedic or dental applications due to their high corrosion resistance and their excellent biocompatibility [5-9], they are not adapted for vascular stents. Indeed, the major drawback of titanium alloys comes from their low ductility (elongation<15%) compared to stainless steels and cobalt-chromium alloys (elongation>40%) [1, 2, 10]. Consequently, there is a huge challenge in developing new biocompatible titanium alloys displaying suitable combination of mechanical properties including high plastic deformation capacity and strain-hardening.

Recently, a new generation of beta titanium alloys dedicated to biomedical applications has been developed. Based on biocompatible alloying elements such as Ta, Nb, Zr and Mo [11], these alloys were designed as low modulus alloys [12] or nickel-free superelastic materials [13-15] mainly for orthopedic or dental applications. β -type titanium alloys (body-centered cubic phase microstructure) take great advantages from their capacity to display several deformation mechanisms as a function of the β -phase stability. Therefore, from low to high β -stabilizer addition, martensitic transformation, mechanical twinning and precipitation hardening can be observed [16, 17]. It was recently highlighted that in metastable β titanium alloys, the strain or stress-induced martensitic (SIM) transformation (into orthorhombic α'' phase) can be tuned to obtain a transformation induced plasticity effect combined with intense deformation twinning [18]. Consequently, this new generation of strain transformable titanium-based alloys that exhibits very large plastic deformation is very interesting for the manufacture of balloon expandable stents.

Thus, the aim of this work is to design a new biocompatible titanium-based alloy possessing high ductility. For that, niobium and molybdenum are chosen as alloying elements. Indeed, Nb is well known to be very good to resist against corrosion in simulated body fluid and presents an excellent biocompatibility [19-21]. Mo is also recognized as biocompatible element [22] and some studies have demonstrated adequate mechanical compatibility and good cytocompatibility of Ti-alloys containing Mo such as Ti-Mo, Ti-Mo-Ta or Ti-Mo-Zr-Fe

[23-26]. The advantage of using Mo is that this element possesses strong β -stabilizer ability on titanium alloys in comparison with Nb, Ta or Zr elements [27, 28] and was showed to enhance both mechanical strength and ductility of metastable β Ti-based alloys [16-18]. Recently, Ti-Nb-Mo alloys have demonstrated excellent biocompatibility in terms of pre-osteoblast behavior during in-vitro experiments [29]. On the other hand, it was demonstrated that very stable passivating oxide films are formed on Ti-Nb-Mo alloy surfaces leading to a very high corrosion resistance in simulated body solution. Particularly, the niobium element was shown to enhance the capacitive characteristics of the passivating oxide layers reducing the release of metallic species, which is also an important property in term of biocompatibility [30]

Our design strategy was based on the “d-electron alloy design method” initially developed by Morinaga [31-33] for titanium alloys. In the present work, we used this model to develop an original Ti-Nb-Mo alloy composition which would have sufficient ductility to be potentially suitable for the manufacture of balloon expendable stents. Once the targeted alloy composition elaborated by melting, its microstructure was investigated by optical microscopy, by electron backscattering diffraction, by X-ray diffraction and by transmission electron microscopy and its mechanical properties was evaluated by tensile tests. A specific investigation of the deformation mechanisms that accommodate the plastic deformation was carried out in this study, particularly by in-situ tensile test under synchrotron beam.

2. Material and methods

2.1. Alloy design and synthesis method

Chemical formulation of the titanium alloy was performed following the “d-electron alloy design method” [33]. This concept consists in providing a physical background to the chemical composition of titanium alloys by connecting the values of two electronic parameters (B_o , which is the covalent bond strength between Ti and alloying elements and M_d , which is the mean d-orbital energy level given in eV) to the chemical stability and the deformation mechanisms of titanium-based alloys. From the starting point of pure Ti, average $\overline{B_o}$ and $\overline{M_d}$ values can be calculated for any alloy. Therefore, as each alloying element possesses its own capacity to stabilize either the α phase or the β phase, regions of phase's stability can be easily localized in a $\overline{B_o}/\overline{M_d}$ map. This map is of great interest because

it can be used as a tool to predict titanium alloys properties, independently from the number of alloying elements. From electronic considerations, both Nb and Mo elements have suitable alloying vectors as indicated in blue in the Bo/Md map in Fig. 1., opening the possibility to trigger various deformation modes upon mechanical deformation. Consequently, a metastable β -type titanium alloy composition containing 16 wt.% of niobium and 8 wt.% of molybdenum (Ti-16Nb-8Mo alloy) was chosen because its calculated \overline{BoBe} (~ 2.83) and \overline{MdMe} (~ 2.425 eV) values (in green in Fig.1.) are right in the mechanically instable zone in which mechanical twinning and/or stress-induced phase transformation can be activated in order to promote extra-plasticity.

In this work, the new Ti-16Nb-8Mo alloy composition was synthesized by the cold crucible levitation melting (CCLM) technique in a CELES induction furnace under a pure argon atmosphere, which was introduced after several cycles of high vacuum pumping. Notable features of CCLM are that it can melt metals with a high melting point, create an alloy of uniform composition and prevent the crucible contamination [34, 35]. The obtained ingots with a weight about 20 g were directly cold rolled into a 0.5 mm plate in thickness, which correspond to a reduction rate of more than 90%. From the metallic plate, tensile test specimens were machined (dog-bone tensile specimens with normalized shape: 3 mm width, 0.5 mm in thickness and a gage length of 15 mm) and disc samples were cut (10 mm diameter and 0.5 mm in thickness) for the mechanical and the microstructural investigations. All specimens and samples were finally solution treated at 850°C for 30 minutes under high vacuum and water quenched in order to restore a fully recrystallized metastable β microstructure from the cold-rolled state. The chemical composition of the new Ti-16Nb-8Mo alloy was checked by EDS analysis and the nominal composition was obtained with less than 0.5 wt.% error, which corresponds to the precision of the EDS analysis method.

2.2. Tensile tests and microstructural analysis methods

Tensile tests until rupture with the strain rate of 10^{-4} s^{-1} were performed with an INSTRON tensile machine to evaluate the mechanical properties of the Ti-16Nb-8Mo alloy. An extensometer was used to measure the strain of the specimens during these tests. On the other hand, an in-situ tensile test was also carried out under optical microscopy by using a GATAN micro tensile tester in order to observe the deformation behavior of the alloy. Prior to the in-situ observations, the tensile specimen was mechanically polished by using several SiC papers

with decreasing grit size and followed by colloidal silica suspension (particles size: 0.05 μm). Moreover, in-situ synchrotron X-ray diffraction (SXR) analysis under tensile test was also conducted in this study. SXR experiments were carried out at the ID-22 high resolution powder diffraction beamline of the European Synchrotron Radiation Facility (ESRF, Grenoble, France) with a 1 mm² X-ray beam size and a 0.35453630 Å wavelength radiation. The in-situ tensile test using a GATAN micro tensile tester (strain rate of 10⁻⁴ s⁻¹) under synchrotron beam was performed by strain increments of 0.5% until 5% of strain and then by strain increments of 5% until 25% of strain. A nine-channel detector was used to collect transmitted diffracted beams and all the SXR profiles between $2\theta=8^\circ$ and $2\theta=18^\circ$ were obtained for each maintained strain. To characterize more precisely the microstructure after deformation, electron back-scattered diffraction (EBSD) analyses were conducted with a scanning electron microscope (Zeiss LEO1530 FEG-SEM operating at 20kV) equipped with a NORDIF EBSD detector. Samples were also observed by transmission electron microscopy (TEM, JEOL 2100Plus TEM operating at 200kV). Thin foils were prepared by twin-jet electro polishing technique using a solution of 4% perchloric acid in methanol.

3. Results

3.1. Tensile tests

Fig. 2. displays a typical engineering stress-strain curve related to the new metastable β Ti-16Nb-8Mo alloy. With this alloy, the yield stress is around 420 MPa, while the tensile strength reaches about 650 MPa. As it can be seen on this figure, large plastic deformation is obtained since more than 45% of elongation (strain at rupture: $\epsilon_r \approx 0.48$) can be reached. It has to be mentioned the excellent cold deformability of this alloy because it could be cold-rolled very easily up to more than 90% of thickness reduction without any damage problem.

From the plastic range of the diagram, a very important strain hardening seems to occur, which probably implies a complex deformation mechanism. In order to evaluate the strain hardening capacity of the alloy, the true stress-strain tensile curve was also drawn and presented in Fig. 3. As it can be seen, the present Ti-16Nb-8Mo alloy exhibits enhanced mechanical properties, particularly a large strain hardening rate, bringing about levels of true stress and true strain at necking of 950 MPa and 0.37, respectively. From true stress-true strain values, the strain hardening behavior in metals or alloys can be described using the

Hollomon model [36, 37]. Indeed, the Hollomon's equation, which is a power law, is given by:

$$\sigma^* = K(\varepsilon^*)^n \quad (1)$$

$$\ln \sigma^* = \ln K + n \ln \varepsilon^* \quad (2)$$

where σ^* is the true stress, ε^* is the true strain, K is the strength coefficient and n is the strain hardening exponent. In the Hollomon's expression, the strain hardening exponent measures the ability of an alloy to strain-harden and larger magnitudes indicate larger degrees of strain hardening. As it can be seen on the diagram in the center in Fig. 3 for which $\ln \sigma^*$ was plotted as the function of $\ln \varepsilon^*$, the Hollomon law fits quite well in the 0.14-0.36 strain range, which constitutes the main part of plastic deformation and a value as high as 0.48 is obtained for the strain hardening exponent.

3.2. In-situ characterization under straining

In order to characterize the deformation mechanisms occurring during straining, a tensile test sample was continuously strained up to 10% of elongation ($\varepsilon=0.1$) and observed by optical microscopy equipped with a video camera. Fig. 4. displays six optical micrographs extracted from the video at different strain. They show clearly the presence of numerous bands of deformation that appear continuously from the initial metastable β -quenched microstructure (Fig. 4.a.). These bands of deformation correspond to twinning formation. It can be clearly observed that the twinning is showed to accommodate very earlier the plastic deformation once the yield strength is reached at about 430 MPa (Fig. 4.b.). At higher elongation, the multiplication of numerous large bands of deformation is continuously activated leading quickly to a massive twinned microstructure (Fig. 4.c-f.). It can be observed that during straining, twins nucleate progressively without growing much to remain very thin (μm in size or less).

In order to characterize if any phase transformation occurs during staining, in-situ X-ray diffraction analyses were conducted under synchrotron beam (SXRD). Fig. 5. displays the SXRD profiles obtained during the in-situ tensile test. The different strains reached are indicated beside each profile. In this figure, only the partial profiles in the angle range 8° - 12° around the main $(110)_\beta$ peak, where the most intense peaks are present, are showed.

Before straining ($\varepsilon=0$), only the $(110)_\beta$ peak is present confirming thus that the alloy is fully beta in its initial metastable quenched state. It can be observed on this figure that a strain-

induced transformation occurs in the alloy during straining. This strain-induced phase corresponds to the martensitic orthorhombic α'' phase, which is well-known to appear in superelastic β -type titanium alloys [13-15]. The diffracted α'' peaks could be well-indexed from the SXRD profiles in this study and the main $(020)_{\alpha''}$, $(111)_{\alpha''}$, $(021)_{\alpha''}$ peaks start to be visible from 1.5% of strain ($\varepsilon=0.015$). On the other hand, it is well evidenced that their intensities continue to increase as the applied strain increases, while the $(110)_{\beta}$ peak intensity decreases at the same time. It is worth noting that the stress-induced martensitic transformation (SIM) occurs in the plastic domain in the present Ti-16Nb-8Mo once the yield strength is reached in contrary to what is observed in superelastic alloys [38].

3.3. Deformed microstructure observations

In this work, the determination of the twinning system was investigated by ~~Electron Backscattering Diffraction (EBSD)~~ Electron Backscattering Diffraction (EBSD). For that, the Ti-16Nb-8Mo alloy was deformed up to 2.5% of strain before the observations. Fig. 6. presents EBSD inverse pole figure maps (IPF) for two different magnifications (Fig. 6.a. and 6.b.) with their corresponding image quality (IQ) maps (Fig. 6.c., ~~and~~ 6.d. and 6.e.). As it can be seen on these maps, the initial microstructure of the alloy exhibits an equiaxed beta-grain microstructure of a few tens of microns. From these maps, the crystallographic orientations of the β grains and their internal very thin twins are clearly observed (colour code of orientations is indicated beside). To ensure statistics, large zone in the deformed specimen was analyzed.

For each grain, the orientations of parent β grains and twins were determined by the Euler angles. The twinning system was then characterized from the existence of poles belonging to the parent crystal and its twin. It can be deduced from the IPF maps that the common rotation axis that transforms a parent crystal into a twinned one is a $\langle 113 \rangle$ direction and the twinning plane, common to a parent crystal and a twin is a $\{332\}$ plane. In this system, the misorientation between a grain and its twin is measured to be 50.5° and corresponds to a $\Sigma 11$ -type boundary. All the $\Sigma 11$ -type boundaries were highlighted in red in the image quality (IQ) maps (Fig. 6.c. and 6.d.). Thus, the $\{332\}\langle 113 \rangle$ twinning system was ~~the only one~~ observed to accommodate the plastic deformation in this alloy. In this deformed microstructure, some very thin bands can also be indexed with the orthorhombic α'' martensitic phase. The boundaries between these α'' -phase thin bands and the β matrix have been highlighted in green in the image quality (IQ) map in Fig. 6.e. Consequently, the stress-induced martensitic

transformation occurring in the present Ti-16Nb-8Mo alloy, which was clearly evidenced by SXRD, is also confirmed by EBSD.

Twins were also observed at higher magnification by transmission electron microscopy (TEM) in this study. Fig. 7. presents TEM images taken from the Ti-16Nb-8Mo microstructure after being deformed up to 2.5% of strain. Fig. 7.a. displays a set of bright-field images in which a twin ~~is~~ is well visible. As it was observed by EBSD, the thickness is sub-micrometric in size as many of the twins formed in this alloy. Fig. 7.b. presents a dark-field image and its corresponding selected area electron diffraction pattern (SAEP) taken in the twin. It can be observed in the β twin the presence of numerous nanoscale precipitates in bright in the dark-field image. These nanoprecipitates correspond to the hexagonal ω phase, which is perfectly indexed by electronic diffraction in the present study and widely observed in this kind of alloys [16, 17, 23, 25, 28]. On the other hand, it has been reported a direct relationship between the presence of the ω phase and the twinning formation in metastable β -Ti alloys [18]. It should be note that the α'' phase could not be observed by TEM in the present study. Indeed, the martensitic α'' phase is mechanically instable and its observation by TEM remains a problem due to the reduced thickness of the TEM sample in which mechanical relaxation occurs. Images in Fig. 7.c., 7.d. and ~~7.e., 7.f. and 7.g.~~ correspond to observations carried out at higher magnification in the zone represented by the white square in Fig. 7.a. On the dark-field image (~~bc~~) and its corresponding selected area electron diffraction pattern taken at the matrix-twin interface (~~ed~~), misorientation of 50.5° can be measured confirming thus that this is the $\{332\}\langle 113\rangle$ twinning system that accommodates the plastic deformation as it was evidenced by EBSD as well. On the other hand, plastic deformation is also observed to be accommodated by dislocations in both β grains and twins as showed in the bright-field image in Fig. 7.~~de~~. In body-centered cubic phase, activated slip systems can be: $\langle 111\rangle\{110\}$, $\langle 111\rangle\{112\}$ or $\langle 111\rangle\{123\}$ [39, 40]. In Fig. 7.~~de~~., the foil was re-tilted to obtain diffraction vector $g=-110$ out of the zone axis to visualize the $\{332\}\langle 113\rangle$ twin interface and the dislocations with Burgers vectors satisfying $g\cdot b \neq 0$. Arrays of dislocations are observed on both sides of the $\{332\}\langle 113\rangle$ twin boundary, i.e. the in-twin dislocation array and geometrically necessary dislocation (GND) array in the beta matrix (labeled in the Fig.7.~~de~~).

4. Discussion

The unusual mechanical properties and deformation mechanisms occurring in the Ti-16Nb-8Mo alloy constitute a new class of strain transformable titanium alloys [17, 18, 41]. Indeed, in addition to the classic dislocation slip, a massive twinning and strain-induced martensitic transformation were also observed to accommodate the deformation in the present alloy unlike other classical titanium alloys used in the biomedical field such as the Ti-6Al-4V ELI alloy for example. It is worth noting that the d-electron alloy design method [31-33] was particularly useful to select the right chemical composition in the view to activate both mechanical twinning and strain-induced phase transformation. Concerning the twinning formation, two twinning systems were commonly observed in β titanium alloys: $\{112\}\langle 111\rangle$ and $\{332\}\langle 113\rangle$ [42, 43]. $\{112\}\langle 111\rangle$ twins were usually observed in stable beta titanium alloys, which have high critical stress for slip due to solution hardening and high Peierls stress. In contrast, $\{332\}\langle 113\rangle$ twinning always occurs in metastable beta titanium alloys and leads to large elongation. Thus, the $\{332\}\langle 113\rangle$ twinning system, which was the only one observed to accommodate the plastic deformation in this alloy and its massive formation can explain the high ductility and strain hardening obtained. Indeed, such massive twinning provides effective obstacles to dislocations motion as it is the case for the well-known TWinning Induced Plasticity (TWIP) steels [44]. But in the present case, a strain-induced martensitic transformation was also observed and contributes also on the high plasticity through a TRansformation Induced Plasticity effect (TRIP). Recent assumptions based on experimental observations suggest that the $\{332\}\langle 113\rangle$ twinning process could be mediated by the formation of the orthorhombic martensitic phase, formed as a martensitic reversion product [45-47]. Nevertheless, other recent study highlighted simultaneous activation of two different deformation modes, the primary TRIP mode on one side, and the hybrid TWIP and secondary TRIP mode on the other side [48]. On the other hand, the observed geometrically necessary dislocation (GND) array associated to the $\{332\}\langle 113\rangle$ twinning formation (Fig. 7.d.) is also thought to play an important role in the strain-hardening behavior of the studied alloy. Due to the intensive multiplication of the twinning bands upon plastic deformation, the GND density and thus the total dislocation density increases continuously as well. As a result, the strong strain-hardening effect exhibited by the studied alloy is contributed by the short-range interaction between moving dislocations and the steadily increasing density of GND. This shows the complexity of the interactions between the various phenomena that accommodate the plastic deformation and how interdependent they could be. This complex deformation mechanism leads to very interesting mechanical properties that can be useful for

the manufacture of balloon expandable stents tanks to the large plasticity observed combined with a strong strain-hardening effect. Indeed, we showed that the strain hardening exponent can reach a value as high as 0.48 with this new biocompatible Ti-16Nb-8Mo alloy, which is more than twice the maximum strain hardening exponent obtained for commercially pure titanium (CP-Ti) or Ti-6Al-4V ELI alloy [49]. On the other hand, this strain hardening exponent value is of the same order of magnitude as those obtained with biomedical stainless steels or Co-Cr based alloys, which are the highest values for metallic materials [50, 51]. It is worth noting that such combination of mechanical properties is never obtained with conventional titanium alloys for which the lack of plastic deformation does not allow their use for the manufacture of stents (risks of fracture during the deployment of the stent or dynamic failure in long-term service.), despite of their excellent biocompatibility compared to stainless steels or Co-Cr based alloys [1, 2, 5-11]. Thus, it appears very clear, as illustrated in Fig. 8. (adapted from [2]), that the new strain transformable Ti-16Nb-8Mo biocompatible alloy exhibiting a TRIP-TWIP behavior that leads to a significant plastic deformation of up to more than 45% of elongation at fracture becomes a competitive titanium-based alloy for stainless steel and Co-Cr alloys for the manufacture of balloon expandable stents.

4. Conclusion

In this work, a new β -type Ti-16Nb-8Mo alloy composition was designed to be adapted for balloon expandable vascular stent technology. With this alloy, a very large plastic deformation (elongation at fracture $> 45\%$) combined with a high strain hardening (strain hardening exponent ≈ 0.48) was obtained by tensile tests contrary to other titanium medical grades. This good mechanical property is due to unusual plastic deformation mechanisms that occur in this alloy. To understand the complex plastic behavior, the alloy was investigated at different scales using different methods of characterization such as EBSD, TEM and SXRD. Observations showed that combination of strain-induced martensitic transformation (into α'' martensitic phase) and massive $\{332\}\langle 113 \rangle$ mechanical twinning formation were taking place during plastic deformation leading to an original TRIP-TWIP (Transformation Induced Plasticity-TWinning Induced Plasticity) effect. Thus, the new highly biocompatible and strain transformable Ti-16Nb-8Mo alloy exhibiting extra-plasticity becomes a very competitive titanium-based alloy for stainless steel and Co-Cr alloys for the manufacture of balloon expandable stents.

References

- [1] G. Mani, M.D. Feldman, D. Patel, C.M. Agrawal, Coronary stents: A materials perspective, *Biomaterials* 28 (2007) 1689-1710
- [2] T. Hanawa, Materials for metallic stents, *J. Artif. Organs* 12 (2009) 73-79
- [3] S.G. Steinemann, Metal implants and surface reactions, *Injury* 27 (1996) 16-22
- [4] I. Gotman, Characteristics of metals used in implants, *J Endourol.* 11 (1997) 383-389
- [5] M. Long, H.J. Rack, Titanium alloys in total joint replacement: A material science perspective, *Biomaterials* 19 (1998) 1621-1639
- [6] M. Niinomi, Recent research and development in titanium alloys for biomedical applications and healthcare goods, *Sci. Technol. Adv. Mater.* 4 (2003) 445-454
- [7] T.A.G. Donato, L.H. de Almeida, R.A. Nogueira, T.C. Niemeyer, C.R. Grandini, R. Caram, S.G. Schneider, A.R. Santos Jr., Cytotoxicity study of some Ti alloys used as biomaterial, *Mat. Sci. Eng. C* 29 (2009) 1365-1369
- [8] M. Geetha, A.K. Singh, R. Asokamani, A.K. Gogia, Ti based biomaterials, the ultimate choice for orthopaedic implants – A review, *Prog. Mater. Sci.* 54 (2009) 397-425
- [9] M. Niinomi, M. Nakai, J. Hieda, Development of new metallic alloys for biomedical applications, *Acta Biomater.* 8 (2012) 3888-3903
- [10] B. O'Brien, J. Stinson, W. Carroll: Initial exploration of Ti-Ta, Ti-Ta-Ir and Ti-Ir alloys: Candidate materials for coronary stents, *Acta Biomater.* 4 (2008) 1553-1559
- [11] S.G. Steinemann, Titanium: the material of choice ?, *Periodontology* 2000 17 (1998) 7-21
- [12] M. Niinomi, Fatigue performance and cyto-toxicity of low rigidity titanium alloy, Ti-29Nb-13Ta-4.6Zr, *Biomaterials* 24 (2003) 2673-2683
- [13] S. Miyazaki, H. Y. Kim, H. Hosoda, Development and characterization of Ni-free Ti-base shape memory and superelastic alloys, *Mater. Sci. Eng.* A438-440 (2006) 18-24
- [14] Y.L. Hao, S.J. Li, S.Y. Sun, R. Yang, Effect of Zr and Sn on Young's modulus and superelasticity of Ti-Nb-based alloys, *Mater. Sci. Eng.* A441 (2006) 112-118
- [15] F. Sun, Y.L. Hao, S. Nowak, T. Gloriant, P. Laheurte, F. Prima, A thermo-mechanical

treatment to improve the superelastic performances of biomedical Ti–26Nb and Ti–20Nb–6Zr (at.%) alloys, *J. Mech. Behav. Biomed. Mater.* 4 (2011) 1864-1872

[16] D. Banerjee, J.C. Williams, Perspectives on Titanium Science and Technology, *Acta Mater.* 61 (2013) 844-8

[17] F. Sun, F. Prima, T. Gloriant, High-strength nanostructured Ti–12Mo alloy from ductile metastable beta state precursor, *Mater. Sci. Eng. A527* (2010) 4262-4269

[18] F. Sun, J.Y. Zhang, M. Marteleur, T. Gloriant, P. Vermaut, D. Lail e, P. Castany, C. Curfs, P.J. Jacques, F. Prima, Investigation of early stage deformation mechanisms in a metastable β titanium alloy showing combined twinning-induced plasticity and transformation-induced plasticity effects, *Acta Mater.* 61 (2013) 6406-6417

[19] H. Matsuno, A. Yokoyama, F. Watari, M. Uo, T. Kawasaki, Biocompatibility and osteogenesis of refractory metal implants Ti, Hf, Nb, Ta, Rh, *Biomaterials* 22 (2001) 1253-1262

[20] Y. Okazaki, S. Rao, Y. Ito, T. Tateishi, Corrosion resistance, mechanical properties, corrosion fatigue strength and cytocompatibility of new Ti alloys without Al and V, *Biomaterials* 19 (1998) 1197-1215

[21] D.M. Gordin, R. Ion, C. Vasilescu, S.I. Drob, A. Cimpean, T. Gloriant, Potentiality of the “Gum Metal” titanium-based alloy for biomedical applications, *Mater. Sci. Eng. C44* (2014) 362-370

[22] E. Eisenbarth, D. Velten, M. M uller, R. Thull, J. Breme, Biocompatibility of beta-stabilizing elements of titanium alloys, *Biomaterials* 25 (2004) 5705-5713

[23] W.F. Ho, C.P. Ju, J.H. Chern Lin, Structure and properties of cast Ti-Mo alloys, *Biomaterials* 20 (1999) 2115-2122

[24] D.M. Gordin, T. Gloriant, G. Texier, I. Thibon, D. Ansel, J.L. Duval, M.D. Nagel, Development of a β -type Ti.12Mo.5Ta alloy for biomedical applications: cytocompatibility and metallurgical aspects, *J. Mater. Sci. Mater. Med.* 15 (2004) 885-891

[25] S. Nag, R. Banerjee, H.L. Fraser, Microstructural evolution and strengthening mechanisms in Ti-Nb-Zr-Ta, Ti-Mo-Zr-Fe and Ti-15Mo biocompatible alloys, *Mater. Sci. Eng. C25* (2005) 357-362

[26] L. Trentania, F. Pelilloa, F.C. Pavesia, L. Ceciliaia, G. Cettab, A. Forlino, Evaluation of

the TiMo₁₂Zr₆Fe₂ alloy for orthopaedic implants: in vitro biocompatibility study by using primary human fibroblasts and osteoblasts, *Biomaterials* 23 (2002) 2863-2869

[27] P.J. Bania, Beta titanium alloys and their role in the titanium industry, *Proceedings of the 13th World Conference on Titanium*, ed. D. Eylon, RR Boyer, D.A Koss (TMS, Warrendale, PA), 1993, pp. 3-14

[28] T. Gloriant, G. Texier, F. Prima, D. Laillé, D.M. Gordin, I. Thibon, D. Ansel, Synthesis and phase transformations of beta metastable Ti-based alloys containing biocompatible Ta, Mo and Fe beta-stabilizer elements, *Adv. Eng. Mater.* 8 (2006) 961-965

[29] P. Neacsu, D.-M. Gordin, V. Mitran, T. Gloriant, M. Costache, A. Cimpean, In vitro performance assessment of new beta Ti–Mo–Nb alloy compositions, *Mater. Sci. Eng. C47* (2015) 105-113

[30] R. Chelariu, G. Bolat, J. Izquierdo, D. Mareci, D.M. Gordin, T. Gloriant, R.M. Souto, Metastable beta Ti-Nb-Mo alloys with improved corrosion resistance in saline solution, *Electrochim. Acta* 137 (2014) 280-289

[31] D. Kuroda, M. Niinomi, M. Morinaga, Y. Kato, T. Yashiro, Design and mechanical properties of new β type titanium alloys for implant materials, *Mater. Sci. Eng. A243* (1998) 244-249

[32] M. Abdel-Hady, K. Hinshita, M. Morinaga, General approach to phase stability and elastic properties of beta-type Ti-alloys using electronic parameters, *Script. Mater.* 55 (2006) 477-480

[33] M. Morinaga, N. Yukawa, T. Maya, K. Sone, H. Adachi, Theoretical design of titanium alloys, *Proceedings of the Sixth World Conference on Titanium*, 1988, pp. 1601-1606

[34] D.M. Gordin, E. Delvat, R. Chelariu, G. Ungureanu, M. Besse, D. Laillé, T. Gloriant, Characterization of Ti-Ta alloys synthesized by cold crucible levitation melting, *Adv. Eng. Mater.* 10 (2008) 714-719

[35] K. Matsugi, T. Endo, Y.B. Choi, G. Sasaki, Alloy design of Ti alloys using ubiquitous alloying elements and characteristics of their levitation-melted alloys, *Mater. Trans.* 51 (2010) 740-748

[36] J.H. Hollomon, Tensile deformation, *Trans. AIME* 162 (1945) 268-290

- [37] R.K. Nutor, N.K. Adomako, Y.Z. Fang, Using the Hollomon model to predict strain-hardening in metals, *Am. J. Mater. Synth. Proc.* 2 (2017) 1-4
- [38] P. Castany, A. Ramarolahy, F. Prima, P. Laheurte, C. Curfs, T. Gloriant, In situ synchrotron X-ray diffraction study of the martensitic transformation in superelastic Ti-24Nb-0.5N and Ti-24Nb-0.5O alloys, *Acta Mater.* 88 (2015) 102-111
- [39] J.W. Christian, Some surprising features of the plastic deformation of body-centered cubic metals and alloys, *Metall. Trans. A* 14 (1983) 1237-1256
- [40] P. Castany, M. Besse, T. Gloriant, In situ TEM study of dislocation slip in a metastable β titanium alloy, *Scripta Mater.* 66 (2012) 371-373
- [41] P. Castany, T. Gloriant, F. Sun, F. Prima, Design of strain-transformable titanium alloys, *Comptes Rendus Physique* 19 (2018) 710-720
- [42] S. Hanada, O. Izumi, Transmission electron-microscopic observations of mechanical twinning in metastable beta titanium alloys, *Metall. Trans. A* 17 (1986) 1409-1420
- [43] E. Bertrand, P. Castany, I. Péron, T. Gloriant, Twinning system selection in a metastable β -titanium alloy by Schmid factor analysis, *Scripta Mater.* 64 (2011) 1110-111
- [44] O. Bouaziz, N. Guelton, Modelling of TWIP effect on work-hardening, *Mater. Sci. Eng. A* 319-321 (2001) 246-249
- [45] M.J. Lai, C.C. Tasan, D. Raabe, On the mechanism of $\{332\}$ twinning in metastable β titanium alloys, *Acta Mater.* 111 (2016) 173-186
- [46] B. Chen, W. Sun, Transitional structure of $\{332\}\langle 113\rangle$ β twin boundary in a deformed metastable β -type Ti-Nb-based alloy, revealed by atomic resolution electron microscopy, *Scripta Mater.* 150 (2018) 115-119
- [47] P. Castany, Y. Yang, E. Bertrand, T. Gloriant, Reversion of a parent $\{130\}\langle 310\rangle\alpha''$ martensitic twinning system at the origin of $\{332\}\langle 113\rangle\beta$ twins observed in metastable β titanium alloys, *Phys. Rev. Lett.* 117 (2016) 245501
- [48] L. Lilensten, Y. Danard, C. Brozek, S. Mantri, P. Castany, T. Gloriant, P. Vermaut, F. Sun, R. Banerjee, F. Prima, On the heterogeneous nature of deformation in a strain-transformable beta metastable Ti-V-Cr-Al alloy, *Acta Mater.* 162 (2019) 268-276
- [49] R.K. Gupta, V.A. Kumar, C. Mathew, G.S. Rao, Strain hardening of titanium alloy Ti6Al4V sheets with prior heat treatment and cold working, *Mat. Sci. Eng. A* 662 (2016) 537-

550

[50] E. Isaac Samuel, B.K. Choudhary, Universal scaling of work hardening parameters in type 316L(N) stainless steel, *Mater. Sci. Eng. A527* (2010) 7457-7460

[51] K. Yamanaka, M. Mori, A. Chiba, Effects of nitrogen addition on microstructure and mechanical behavior of biomedical Co-Cr-Mo alloys, *J. Mech. Behav. Biomed. Mater.* 29 (2014) 417-426

Journal Pre-proof

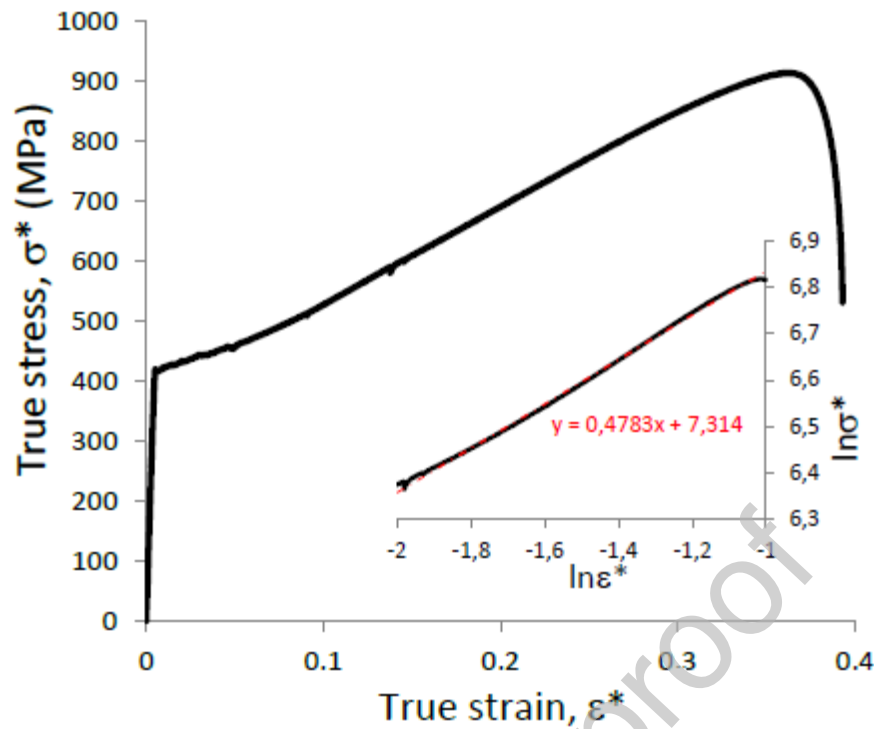


Fig. 3. True stress-strain tensile curve of the Ti-16Nb-8Mo alloy. At the center, a linear relationship between $\ln\sigma^*$ and $\ln\epsilon^*$ is evidenced in accordance with the Hollomon law.

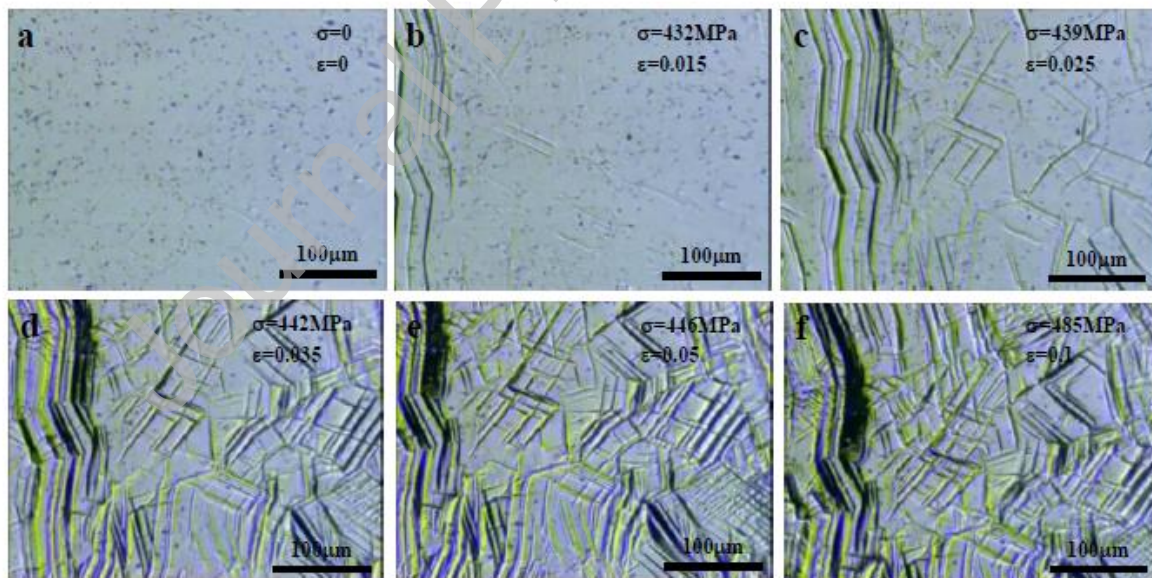


Fig. 4. Optical microscopy images from the video during in-situ tensile test that show the twinning formation in the Ti-16Nb-8Mo alloy: (a) initial state; (b) at 0.015 strain; (c) at 0.025 strain; (d) at 0.035 strain; (e) at 0.05 strain and (f) at 0.1 strain.

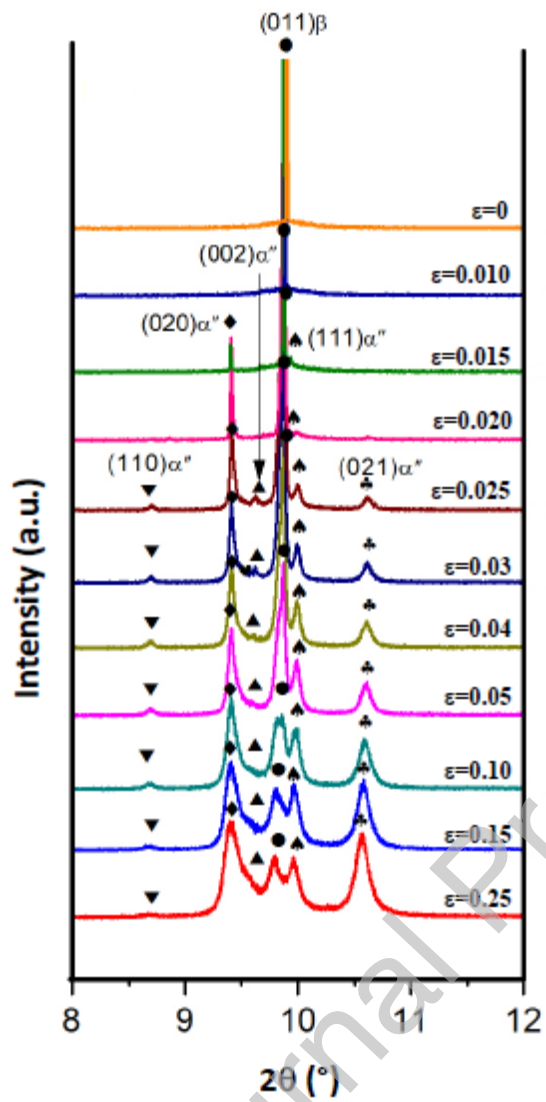


Fig. 5. SXR D profiles obtained during in-situ tensile test (the different strains are indicated beside each profile).

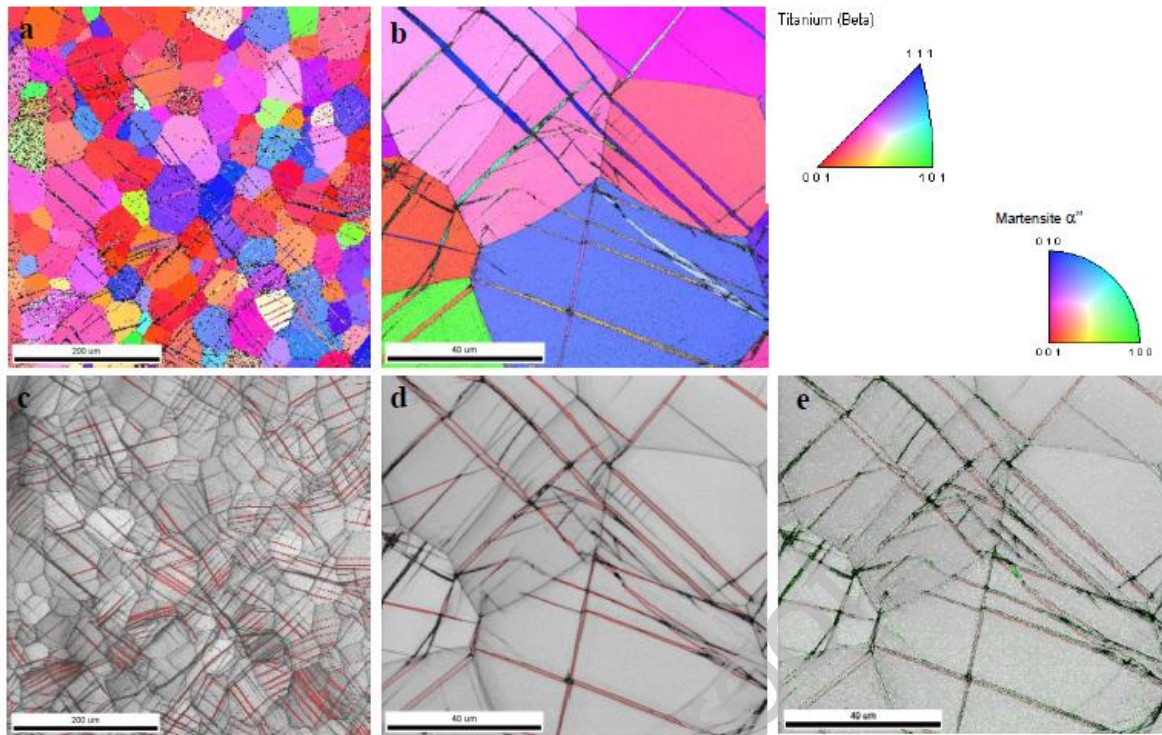


Fig. 6. EBSD inverse pole figure (IPF) maps of the deformed Ti-16Nb-8Mo for two different magnifications (a and b) and their corresponding image quality (IQ) maps (c, d and e).

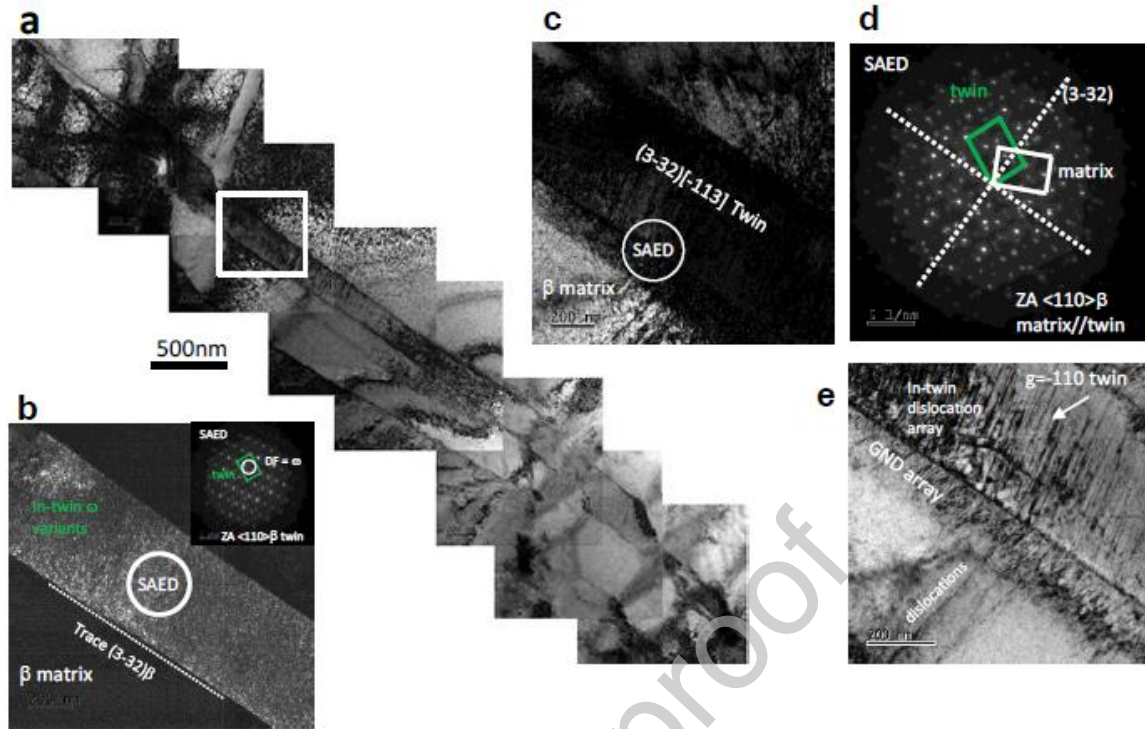


Fig. 7. TEM micrographs from the deformed Ti-16Nb-8Mo alloy. (a) set of bright-field images; (b) dark-field image and its corresponding SAED pattern taken in a twin; (c) dark-field image of a $\{332\}\langle 113\rangle$ twin; (d) SAED pattern at the matrix-twin interface; (e) bright-field image of dislocation array.

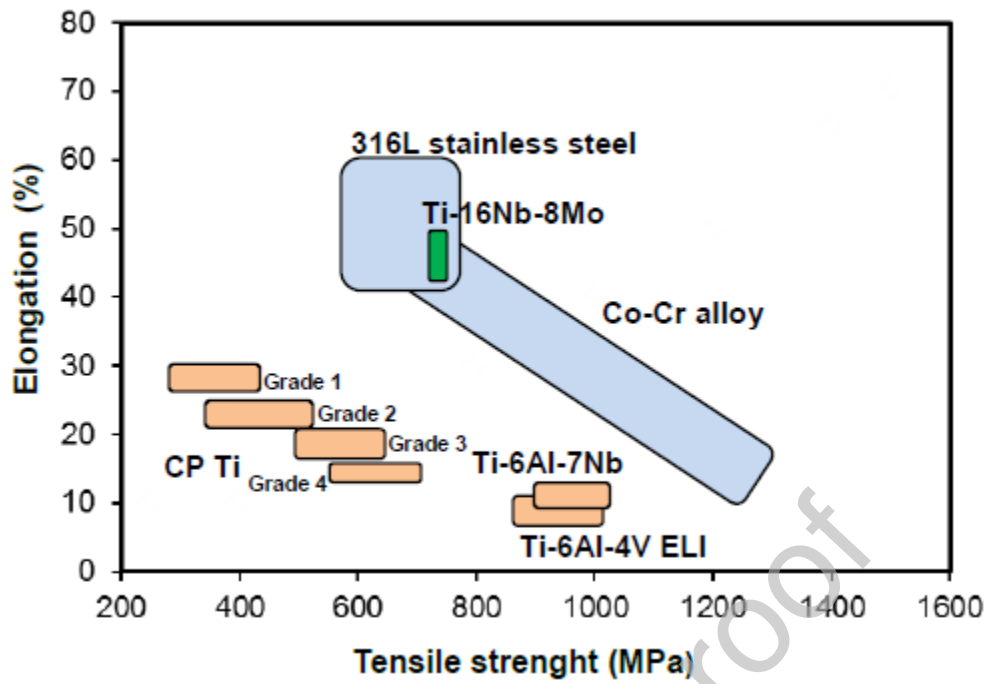


Fig. 8. Tensile strength and elongation balance of various alloys for medical use (adapted from [2]). The new Ti-16Nb-8Mo alloy is highlighted in green.

Declaration of interests

The authors declare that they have no known competing financial interests or personal relationships that could have appeared to influence the work reported in this paper.

The authors declare the following financial interests/personal relationships which may be considered as potential competing interests:

Journal Pre-proof

Graphical abstract

